

A High Content Screen in Macrophages Identifies Small Molecule Modulators of STING-IRF3 and NFκB Signaling

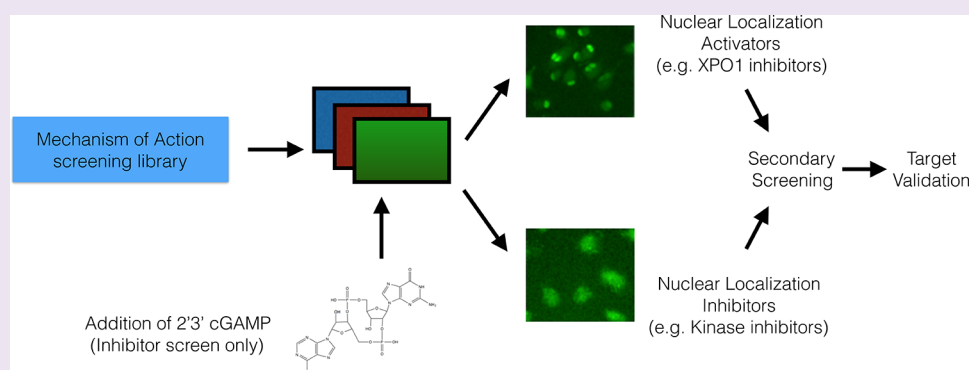
Peter D. Koch,^{*,†,‡} Howard R. Miller,[§] Gary Yu,[§] John A. Tallarico,[§] Peter K. Sorger,^{†,‡} Yuan Wang,[§] Yan Feng,[§] Jason R. Thomas,[§] Nathan T. Ross,[§] and Timothy Mitchison^{†,‡}

[†]Department of Systems Biology, Harvard Medical School, 200 Longwood Ave., Boston, Massachusetts 02115, United States

[‡]Laboratory of Systems Pharmacology, Harvard Medical School, 200 Longwood Ave., Boston, Massachusetts 02115, United States

[§]Chemical Biology and Therapeutics, Novartis Institutes for Biomedical Research, 181 Massachusetts Ave., Cambridge, Massachusetts 02139, United States

S Supporting Information



ABSTRACT: We screened a library of bioactive small molecules for activators and inhibitors of innate immune signaling through IRF3 and NFκB pathways with the goals of advancing pathway understanding and discovering probes for immunology research. We used high content screening to measure the translocation from the cytoplasm to nucleus of IRF3 and NFκB in primary human macrophages; these transcription factors play a critical role in the activation of STING and other pro-inflammatory pathways. Our pathway activator screen yielded a diverse set of hits that promoted nuclear translocation of IRF3 and/or NFκB, but the majority of these compounds did not cause activation of downstream pathways. Screening for antagonists of the STING pathway yielded multiple kinase inhibitors, some of which inhibit kinases not previously known to regulate the activity of this pathway. Structure–activity relationships (SARs) and subsequent chemical proteomics experiments suggested that MAPKAPK5 (PRAK) is a kinase that regulates IRF3 translocation in human macrophages. Our work establishes a high content screening approach for measuring pro-inflammatory pathways in human macrophages and identifies novel ways to inhibit such pathways; among the targets of the screen are several molecules that may merit further development as anti-inflammatory drugs.

The innate immune system has evolved to include many signaling pathways that detect pathogens.^{1–4} Mutations in these pathways controlling the innate immune system cause several diseases: hyperactivity has been linked to inflammatory and autoimmune diseases,^{2–4} and abnormally low activity has been linked to susceptibility to infectious disease, and possibly even cancer.^{5,6} Several inhibitory drugs are already approved or in development for inflammatory diseases,⁷ while interest in pathway agonists has grown with the recent successes of immuno-oncology checkpoint inhibitors.⁸

An innate immune response is typically triggered by binding of a pathogenic associated molecular pattern (PAMP) to a receptor. Different pathways are tailored to recognize specific PAMPs. For example, lipopolysaccharide (LPS), a component of bacterial cell membrane, is recognized by Toll-like-receptor 4 (TLR4), which leads to NFκB translocation into the nucleus.^{1,2} Cytosolic dsRNA, a feature of viral infection, is recognized by

the receptors, MDAS and RIG-I, which leads to translocation of the transcription factor IRF3 into the nucleus.^{1,2} Of particular interest is the recently discovered cGAS-STING pathway, which detects cytosolic DNA^{3,9} (Figure 1a). Cytosolic dsDNA, which is another feature of viral infection, binds to cGAS (MB21D1), which cyclizes intracellular GTP and ATP to form the second messenger 2'3'-cGAMP. 2'3'-cGAMP binds to a receptor, STING (Stimulator of Interferon Genes). 2'3'-cGAMP-liganded STING activates the kinase TBK1, which phosphorylates the transcription factor IRF3. STING activation has been reported to activate the NFκB pathway as well,³ though this aspect of STING biology has not been thoroughly explored. In the nucleus, both IRF3 and NFκB are capable of

Received: December 12, 2017

Accepted: March 9, 2018

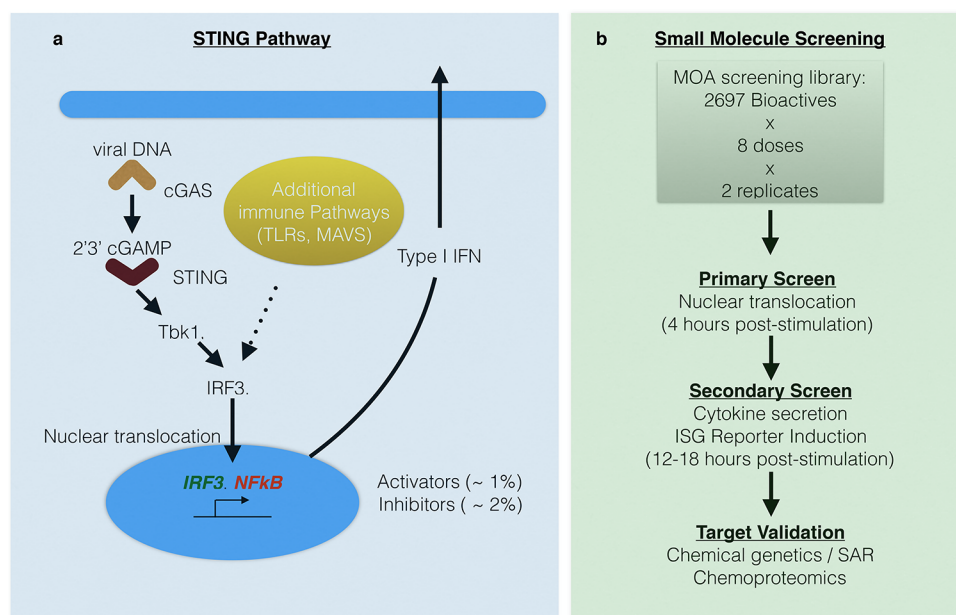


Figure 1. (a) Brief schematic of antiviral signaling pathways. Viral DNA binds to cGAS, which produces 2'3'-cGAMP. 2'3'-cGAMP binds to STING, which activates the transcription factor IRF3 *via* the kinase Tbk1. NFkB is also activated, likely by the IKK kinases, though this effect has not been as thoroughly studied. Other antiviral pathways also activate IRF3 and NFkB, by a similar mechanism. The transcription factors promote the expression of cytokines, which ultimately get secreted. (b) Schematic of the screening approach. In the primary screen, small molecule hits were identified in primary macrophages by an IRF3/NFkB nuclear translocation screen. Secondary screens focused on whether these hits modulated gene expression at later time points, and subsequent work focused on identifying the mechanism of action of these hits.

activating the expression of many antiviral and pro-inflammatory genes. Multiple research groups have described the identification of additional regulatory molecules,^{3,10} but at this point, the cGAS-STING-TBK1-IRF3 axis appears to be the most validated and prominent.

The STING-IRF3 pathway is of considerable therapeutic interest. Direct STING agonists are currently in clinical trials in cancer, based on the hypothesis that activation of the STING pathway will trigger antitumor innate immune responses.^{11–14} Inappropriate activation of the STING pathway has been implicated in sterile inflammatory disease, notably the inherited condition “STING-associated vasculopathy with onset in Infancy (SAVI).”⁴ STING activation has also been proposed as a contributing mechanism in a variety of chronic inflammatory diseases such as lupus and arthritis.¹⁵ Thus, inhibitors of the STING pathway may be of value in treating inflammatory disease. Known pathway components druggable by small molecules include cGAS, STING, and TBK1, and it would be useful to identify additional targets.

Phenotypic assays have a track record of success in discovering novel signaling molecules, even in well-characterized signaling pathways.^{16,17} Previous phenotypic screens on innate immune pathways have traditionally relied on immortalized cell culture models, often coupled with artificial reporters.^{18,19} These systems are convenient surrogates for dissecting signaling biology but fall well short of fully recapitulating STING activity as observed human disease. To maximize physiological relevance, we screened in primary human macrophages and used multiple donors in follow-up experiments. We measured localization of transcription factors, IRF3 and NFkB, in cells exposed to a collection of approximately 2700 bioactive small molecules comprising a “Mechanism of Action” library (MOA; Figure 1b). This library was carefully curated using bio- and cheminformatic criteria and

consists of biochemically well-characterized molecules that interact with protein targets having diverse biological functions.²⁰ All compounds were screened at eight doses, ranging from 100 μ M to 31.6 nM. Screening in dose helps us more confidently discriminate true hits from false positives. Our primary goal was to identify STING pathway regulators, but changes in IRF3 and NFkB nuclear localization can result from other innate immune pathways. As such, any probes and/or regulatory nodes identified in our screen might be relevant to other immune pathways.

We report the results of both an activator and inhibitor screen (Figure 1). In the activator screen, we treated macrophages with compound alone, and measured IRF3 and NFkB nuclear localization after 4 h of treatment. This screen should identify activators of the STING pathway and other innate immune pathways, such as TLR4 and RIG-I. In the inhibitor screen, we pretreated macrophages with the MOA library compounds for 4 h and then added the naturally occurring STING agonist, 2'3'-cGAMP, for another 4 h. This screen is more STING-centric, as we identify molecules that modulate the cellular response to 2'3'-cGAMP. For both screens, we then further profiled the hits in a secondary screen by measuring their effects on secretion of pro-inflammatory cytokines, using sandwich ELISAs.

RESULTS

Validation and Summary of the Activator Screen.

High content screens were executed in 1536 well plates using adherent macrophages made by differentiation of human CD14+ monocytes with M-CSF. We imaged IRF3 and NFkB in the same wells by immunofluorescence and stained nuclei to provide a mask for quantification of nuclear translocation. Validation of the activator screen is shown in Figure 2, where each dot represents the average of approximately 1250 cells in

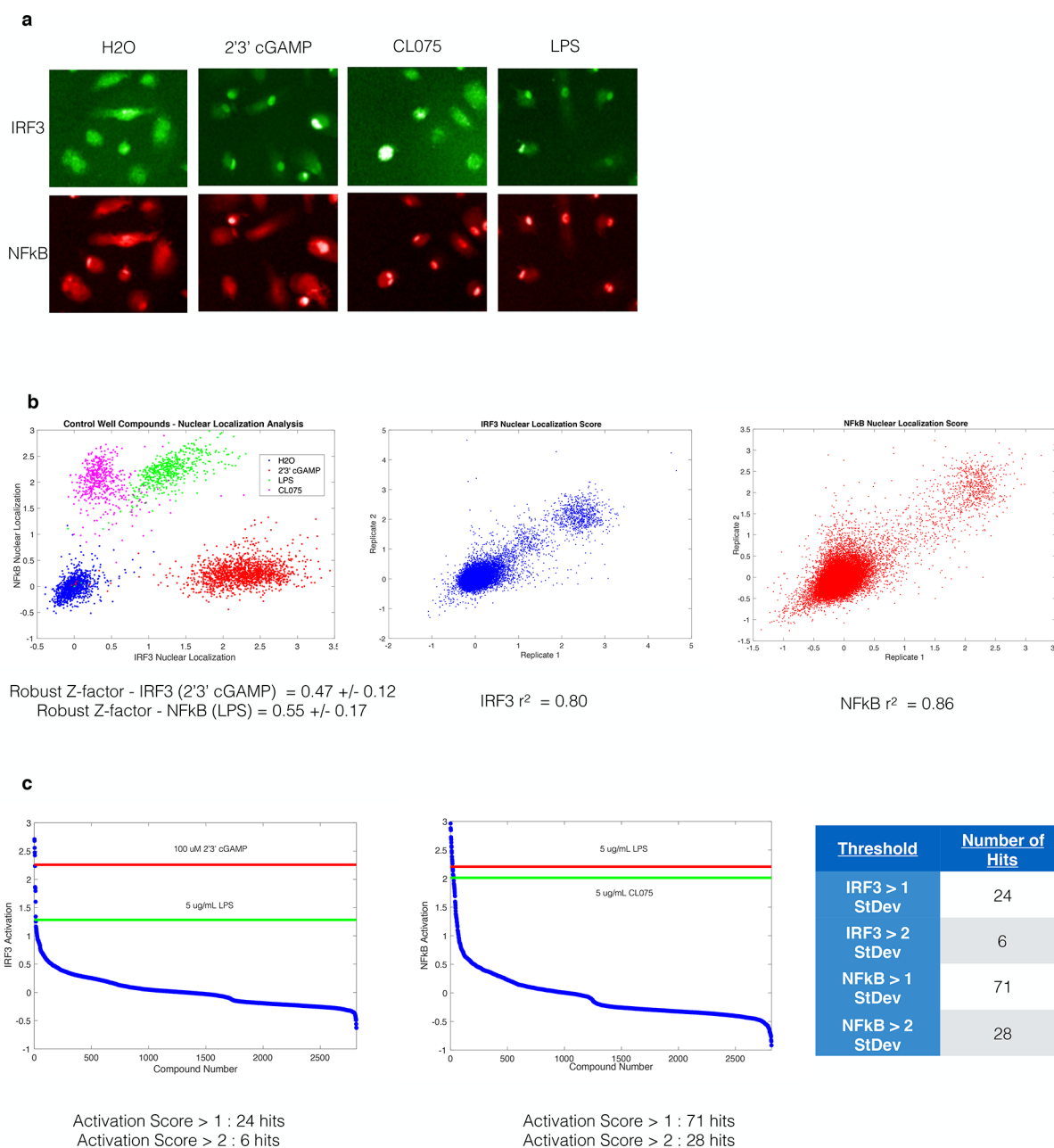


Figure 2. Summary of activator screen. (a) Representative images from control group wells. cGAMP activates IRF3, CL075 activates NFkB, and LPS activates both. (b) Quantification of IRF3 and NFkB nuclear fractions for control groups (left). Replicate analysis for IRF3 scores (middle) and for NFkB scores (right). (c) Waterfall plot for IRF3 and NFkB activators. Scores for each compound were computed by taking the maximum effect achieved out of the doses considered. The hit rates were low, especially for IRF3 activators.

one well. To assess how robustly this assay could distinguish IRF3 translocation from NFkB translocation, cells were treated with either the STING specific pathway agonist 2'3'-cGAMP, 3'3'-cGAMP (a linkage isomer, with weaker activity on STING), a TLR 7/8 agonist CL075, or LPS, a TLR4 agonist, which activates both pathways. Treatment groups were well separated, with a robust Z-factor near 0.5 for both IRF3 and NFkB channels, and replicates were well-correlated (Figure 2a,b). Most plates had outlier control wells, but as we included several replicates per control (at least 16 wells), their effect on screen quality was minimal. Not shown in Figure 2 is 3'3'-cGAMP, which only minimally increased IRF3 nuclear fractions. 3'3'-cGAMP is a nonendogenous cyclic dinucleotide, with much weaker binding affinity for STING. We suspect its

failure to more robustly increase IRF3 nuclear levels, at an early time point, could be due to weaker binding and/or cell permeability. NFkB was translocated into the nucleus slightly above baseline following 2'3'-cGAMP treatment, suggesting that 2'3'-cGAMP weakly activates NFkB at an early time point. This finding contrasts with pathway diagrams that draw IRF3 and NFkB as equal outputs from activated STING.³ Our data suggest that in human primary human macrophages, the magnitude or kinetics of IRF3 and NFkB activation by STING vary.

Our computational pipeline easily enables examination of phenotypes at a single cell level (Figure 3). In the case of 2'3'-cGAMP stimulation, vehicle control wells exhibited IRF3 nuclear fractions that were centered around 0.2–0.3. Some

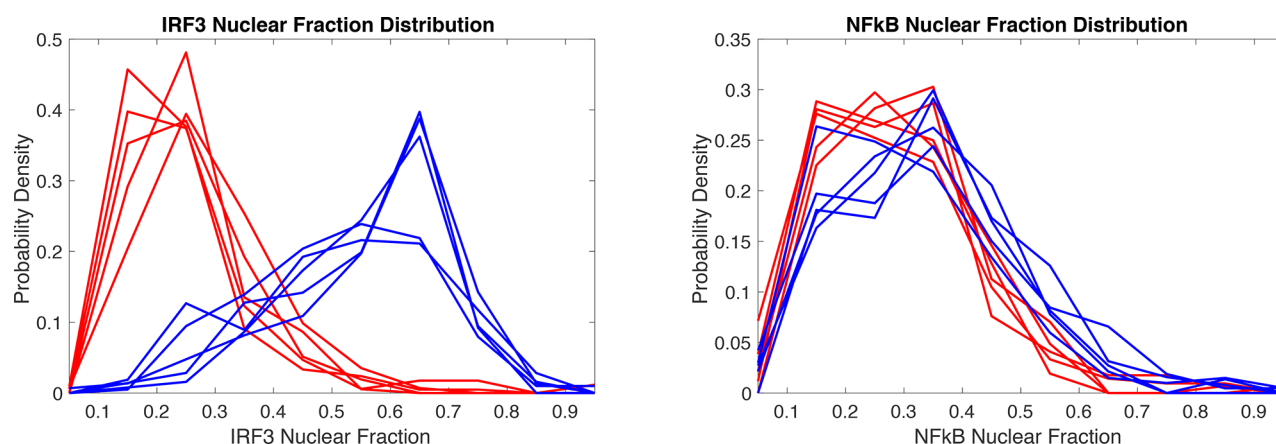


Figure 3. Distributions of IRF3 and NFkB nuclear fractions for five cGAMP treated wells (blue) and H₂O treated wells (red). Each line represents the distribution in a single well.

2′3′-cGAMP treated wells displayed distributions that were sharply peaked around 0.6–0.7. Other wells had distributions that were nearly flat, reflecting heterogeneity in the cellular population.

The hit rate for IRF3 translocators was low (Figure 2c). Only six hits scored higher than 2 standard deviations above the H₂O control (0.22%), and 24 hits, about 1% of the library, scored above 1 standard deviation above the control. The NFkB hit rate was higher, with 28 molecules scoring above 2 standard deviations above the control, and 71 molecules scoring 1 standard deviation above the control, perhaps reflecting more diverse inputs into this pathway.

We chose to follow up on IRF3 activators, as there is potential clinical value in immuno-oncology in small molecule inducers of IRF3-dependent cytokines such as IFN β and CXCL10. To test the extent to which our hits identified by changes in IRF3 translocation were truly “2′3′-cGAMP-like” in their effects, we exploited the high content nature of the screen to extract 36 image-based features of hit and control compounds. Features included nuclear and cytoplasmic intensities, nuclear and cytoplasmic texture features, and morphology parameters, for both IRF3 and NFkB stains (see Methods). These features were used to train a quadratic support-vector machine (SVM) that classified compound-treated wells as either “H₂O-like,” “2′3′-cGAMP-like,” “3′3′-cGAMP-like,” “LPS-like,” or “CL075-like.” This analysis is described in more detail in the Methods and Supporting Information (SI Figure 1) and helped to characterize the translocation phenotype; it yielded 30 “2′3′-cGAMP-like” compounds of interest, to which we added six additional IRF3 activators out of biological interest (Table 1). No particular biological mechanisms seemed enriched, but multiple nuclear export inhibitors scored, suggesting that our screen did identify valid hits.

IRF3 Nuclear Translocation Is Necessary but Not Sufficient for Downstream Pathway Activity. Our secondary assay for pathway activators was secretion of the pro-inflammatory, IRF3-dependent chemokine IP-10 (CXCL10; Supporting Information Figure 2). As we aimed to identify both new signaling proteins and potential therapeutics, we decided to directly screen hits in the secondary assay, as the number of hits we had was reasonably small, and the effect on gene expression needed to be assessed. To our surprise, most primary screen hits did not reliably induce secretion of IP-10. This shows that nuclear import of IRF3 is

not sufficient to activate gene expression. The diverse MOAs of compounds scoring positive in the high content assay and negative for gene expression suggests that multiple mechanism can promote IRF3 translocation without downstream gene expression. One obvious mechanism is inhibition of nuclear export by compounds 10 and 11 (Table 1); these compounds inhibit XPO1, which has been previously implicated as the exporter for IRF3.²¹ How other compounds in Table 1 act is less clear. Two compounds, annotated as ubiquitin protease inhibitors (compounds 33 and 36), should promote ubiquitination, which is often an activating process of innate immune pathways.^{22,23} They did not promote secretion of IP-10, although in two out of three donors, they did induce TNF α secretion in a dose dependent manner (Supporting Information Figure 3). This finding may be coincidental though, as TNF α is driven by NFkB, not IRF3. Nonetheless, it opens the possibility that deubiquitinase inhibitors may have utility in immuno-oncology.

IRF3 Pathway Action by Zinc Chelation. The Zn²⁺ chelator TPEN scored positive in duplicate, and it induced secretion of IP-10 to levels comparable to those of the positive controls 2′3′-cGAMP and LPS. As such, it was the highest-confidence true positive from the activator screen. To further investigate how TPEN might function, we tested its effects in multiple cell types and assays. TPEN induced the activity of a stably transfected luciferase reporter sensitive to IRF3 activation in PMA-primed THP1 cells, a cell line model of macrophages, as well as a murine macrophage line, RAW264.7 (Figure 4a). To test whether this effect was due to chelation of Zn²⁺, we precomplexed TPEN with ZnCl₂ and observed that the TPEN-Zn complex did not cause activation of the same reporter in RAW cells (Figure 4a). This implies pathway activation by removal of Zn²⁺ from intracellular stores, or perhaps of another ion that is similar to Zn²⁺ in binding tightly to TPEN. Our data support a published hypothesis that intracellular zinc represses IRF3 signaling.²⁴ At higher concentrations TPEN was cytotoxic (as measured by Cell-Titer-Glo; Figure 4b), and thus, its window of activity as an inducer of IRF3 dependent genes is narrow. Upon further testing in primary human cells from additional donors, TPEN did not score by cytokine secretion assays. Given its narrow range of nontoxic activity and donor-specific effects, TPEN is not likely to have therapeutic value. These toxicity findings also open the possibility that some of the small molecule hits in

Table 1. continued

hit number	annotated gene/MOA	PubChem CID	SMILES	Common name
30	NFKB pathway inhibitor	5353431	<chem>CC1=CC=C(C=C1)[S](=O)(=O)C=C\C#N</chem>	Bay 11-7082
31	CALCRL antagonist	6918567	<chem>CN(C(=O)C1=CC(=C(C=C1)[S](=O)C2=NC=CS2)[N+][O-])C3=CC=CC=C3C</chem>	SB 268262
32	STAT3 inhibitor	4253236	<chem>O=C(NC1=NN=C(O)C2=CC=CO2)C3=CC(=NC4=CC=CC=C34)C5=CC=CC=C5</chem>	STX-0119
33	CASP3 inhibitor, CTSB inhibitor	292929	<chem>O=C1C2=CC=CC=C2C3=NC(=C(N=C13)C#N)C#N</chem>	9-oxo-9H-indeno[1,2-b]pyrazine-2,3-dicarbonitrile
34	PTPRC	6763	<chem>O=C1C(=O)C2=CC=CC=C2C3=CC=CC=C13</chem>	9,10-phenanthrenequinone
35	ORAI1 blocker	58295621	<chem>OC(=O)C1=C(NC(=O)C2=CC=CC=C(O2)[N+][O-])=O)SC=C1C3=CC=C(C(Cl)C=C3</chem>	SCHEMBL1952374
36	USP7 inhibitor	2819993	<chem>CC(=O)C1=CC(=C(S1)SC2=C(Cl)C(=CC=C2)Cl)[N+][O-]=O</chem>	882257-11-6

^aCompounds 1–30 were selected as cGAMP-like at 10 μ M or less. Compounds 31–36 were selected IRF3 inducers from the preliminary analysis.

Table 1 may activate IRF3 but poison downstream gene expression.

Validation and Summary of the Inhibitor Screen.

Validation of the pathway inhibitor screen is described in Figure 5. Control groups are distinct as shown in Figure 5a,b. The robust Z-factor for the inhibitor screen was also around 0.5, although in this calculation, we ignored a plate of cells that displayed image analysis segmentation errors in a few wells. Control groups were well separated, and replicates were correlated (Figure 5b). Two known TBK1 kinase inhibitors, BX795 and MRT67307, blocked IRF3 nuclear translocation. Both compounds inhibit multiple kinases, and the stronger effect of BX795 might be due to its broader target spectrum.²⁵ Interestingly, LPS, which was simply used as a control for activation of NFkB, appeared to repress IRF3 signaling in combination with 2'3'-cGAMP (Figure 5b).

The hit rate for the inhibitor screen was much higher than for the activator screen, with 14% of the library blocking IRF3 activation to a level 3 standard deviations below the 2'3'-cGAMP control. A total of 24 hits (~ 1%) block IRF3 activation to a level below the BX795 control, and 48 hits (~ 2%) block IRF3 activation to a level below the MRT67307 control (Figure 5c). While toxicity can contribute to a higher inhibitor hit rate, we do not think it is significant enough at the time point to fully account for the higher value. We think that the higher rate likely reflects more avenues to block signal transduction than to activate it. For example, as innate immune pathways utilize kinases to mediate signaling, there are several proteins one can target with multiple drugs, potentially offering more ways to inhibit the pathway.

In selecting pathway inhibitors, we utilized the high content information provided by the screen, though our approach was simpler, involving selecting compounds close to the H₂O control in the multidimensional principal component space (see Methods, Supporting Information Figure 4). We selected 55 compounds from the primary inhibitor screen (Table 2) and prioritized 40 for retesting, based on availability and likely biological interest.

We observed clear enrichment of kinase inhibitors in the hit list, and they represented approximately 65% of pathway inhibitor hits (Figure 5d). The pan-kinase inhibitor, staurosporine, which is an inhibitor of TBK1, was one of the top scoring hits. Apart from kinase inhibitors, there also was enrichment of natural product antibiotics. Brefeldin A, a known STING pathway antagonist, also scored strongly. Upon activation, STING, which is an ER membrane protein, traffics to the perinuclear region when it is activated,⁴ and brefeldin A is thought to block this transport. Multiple ATP6 VIA inhibitors also scored very potently. Due to availability, we substituted bafilomycin A1 and concanamycin A, known ATP6 VIA inhibitors, as tool compounds in future assays.

While our focus was on finding pathway inhibitors, it is worth noting that the screen had the capability to find pathway potentiators as well (Figure 5c). For example, both MG132 and bortezomib, proteasome inhibitors which block NFkB activation, enhance IRF3 activation. This result also has been previously reported.²⁶ It is unlikely these compounds promote gene expression at later time points, given data from the activator screen showing that nuclear location of IRF3 is not sufficient for downstream gene activation.

Most Pathway Inhibitors Block Downstream STING Signaling. We again used IP-10 secretion as a secondary assay for compounds scoring in the translocation assay. We retested

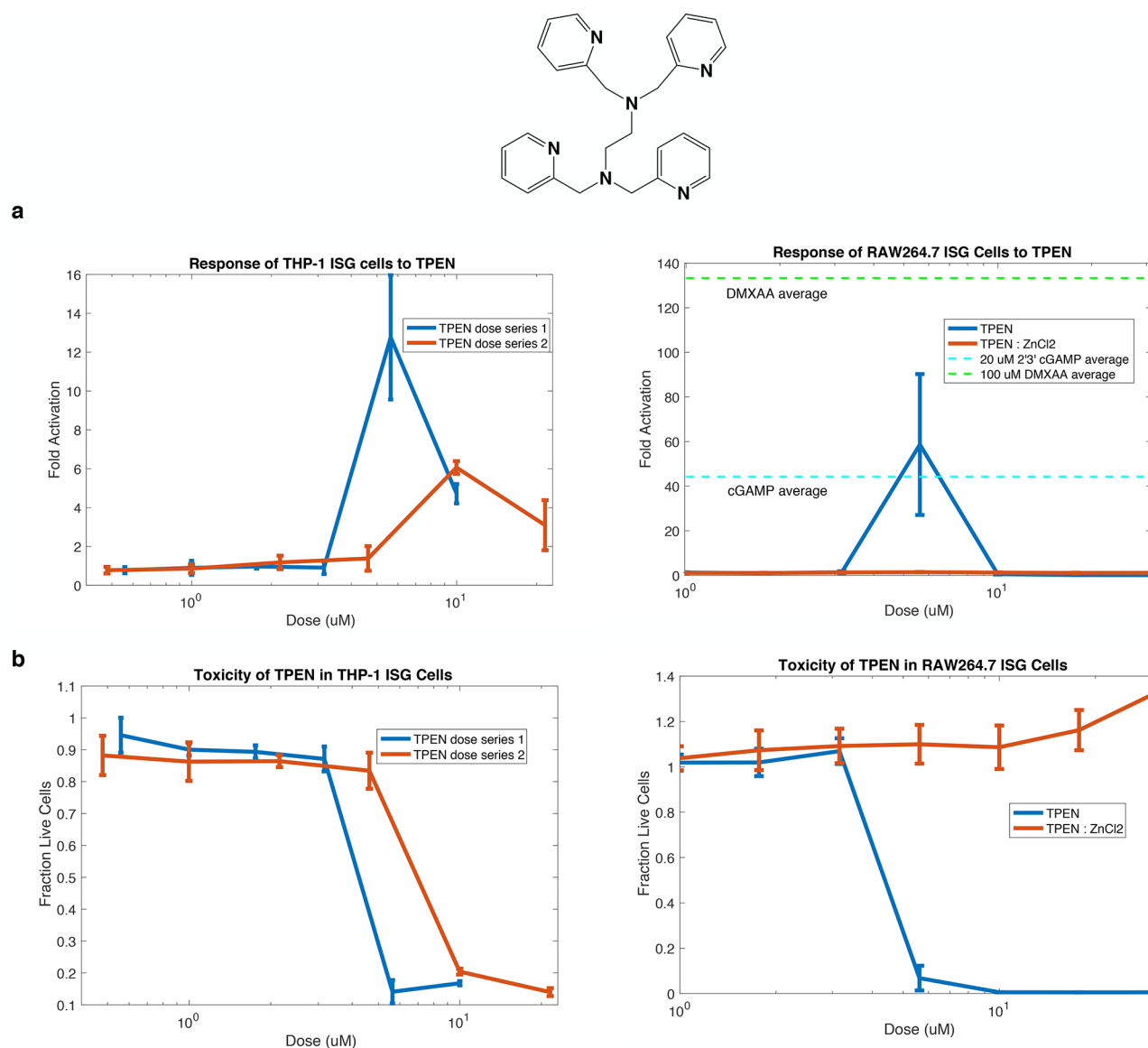


Figure 4. Retest of TPEN in THP-1 ISG and RAW264.7 ISG cells. (a) TPEN induces secretion of the ISG driven Lucia construct, but to different extents in two different cell lines. Activity of TPEN in RAW264.7 cells appears to be due to chelation of intracellular zinc. In RAW cells, the dose response is narrowly peaked as in the primary macrophage IP-10 ELISA secondary screen (Supporting Information Figure 2). (b) Induction of the ISG reporter correlates with toxicity in both cell lines. Error bars correspond to $N = 3$ technical repeats for THP-1 cells and $N = 2$ for RAW cells.

40 compounds, based on interest and availability, and found that most primary screen hits blocked IP-10 secretion by ELISA assays (Supporting Information Figure 5). To test if the effect was due to pathway inhibition or to more general cellular toxicity, we also measured percent of living cells by Cell-Titer-Glo (CTG). The majority of compounds had little or no toxicity at the relevant time point (0–30% reduction in ATP levels by CTG assay). Only four compounds (compounds 1, 9, 24, and 32) exhibited greater than 50% cell killing at one more doses. It is worth noting that toxicity does not mean that these compounds are false positive from the primary screen but does suggest that such compounds are likely to have limited therapeutic value. In Supporting Information Figure 5, we normalize the amount of the pathway inhibition to the amount of remaining cells on the plate. Most compounds show inhibition of the STING pathway, even accounting for toxicity.

Annotated kinase inhibitors comprised the majority of compounds that could be confirmed using the secondary (IP-

10 secretion) assay, further enforcing our view that kinase inhibitors are among the most promising tools to inhibit STING-dependent signaling. Of the nonkinase inhibitors, we were intrigued by both bafilomycin and concanamycin, which blocked pathway activation at low doses but unexpectedly potentiated pathway activity at higher doses. We did not delve into this further but note that a recent report²⁷ implicated a negative regulatory role of ATP6 VIA, consistent with our finding.

Compounds that did not block IP-10 secretion may have been false positives from the primary screen, although it is also possible that donor variability is a confounder. For example, two EHMT inhibitors (compounds 23 and 49) scored in the primary screen, but compound 23 did not score in the secondary screen.

Kinase Inference from Primary Screen Data. Preliminary analysis of kinase inhibitor specificity suggested that TBK1 is not the only kinase required for STING-IRF3 signaling in

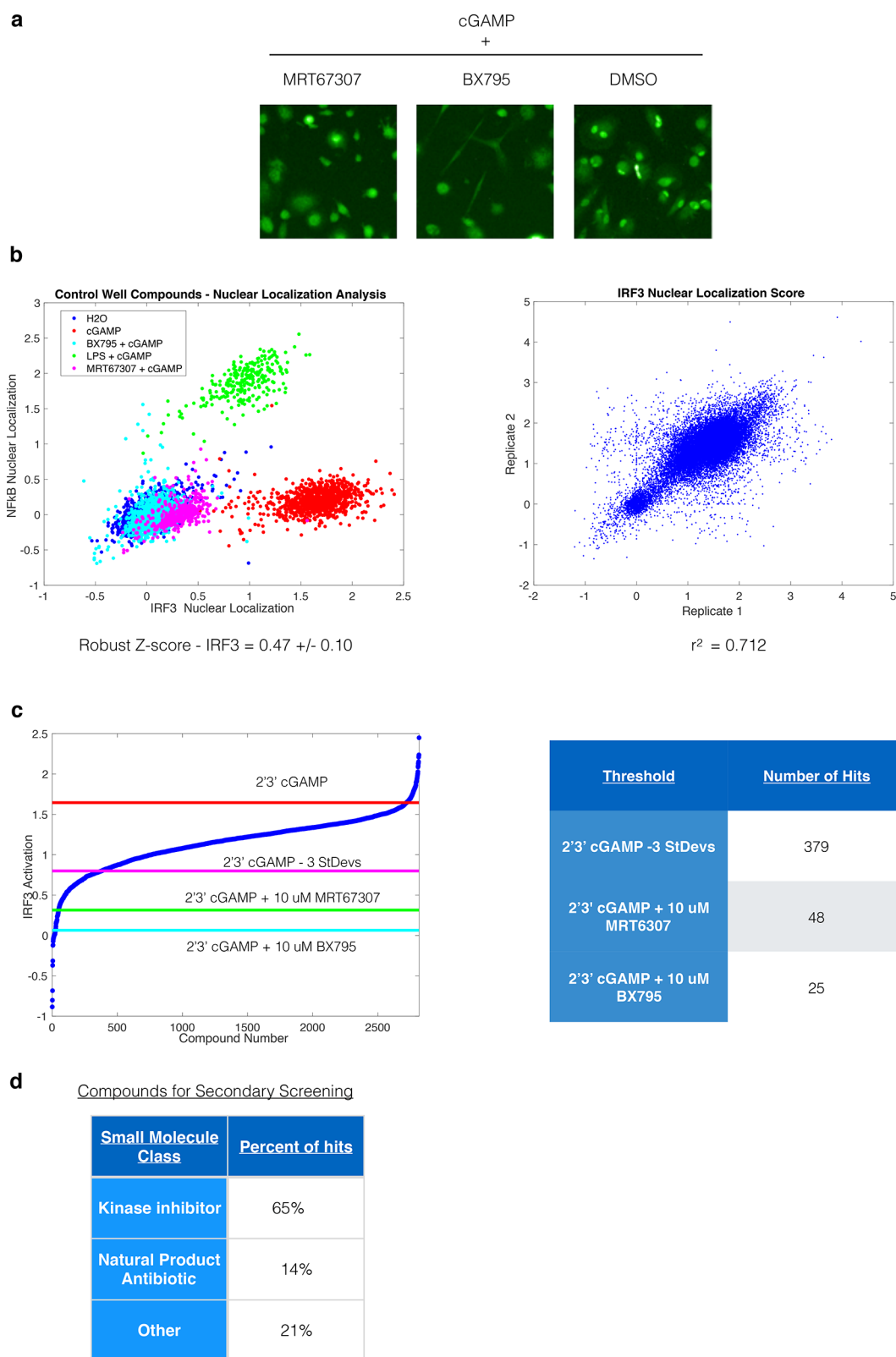


Figure 5. Summary of the inhibitor screen. (a) Sample images from control groups. The Tbk1 inhibitors, BX795 and MRT67307, block IRF3 nuclear fraction. (b) Quantification of control group IRF3 fraction (left) and replicate analysis (right). (c) Waterfall plot for the inhibitor screen. Score for each compound was computed by taking the maximum effect. Both inhibitors and potentiators can be resolved. (d) Summary of chemical class for inhibitors shown in Table 2. Kinase inhibitors and natural product antibiotic are enriched.

human macrophages. We therefore used informatic approaches to identify other kinases required for STING-IRF3 signaling based on the known specificity of the library compounds. The

primary challenge we faced is polypharmacology. Most of the hits were either not potent and/or selective enough to assume that its efficacy target(s) is (are) the nominal (primary)

Table 2. List of Selected Antagonists^a

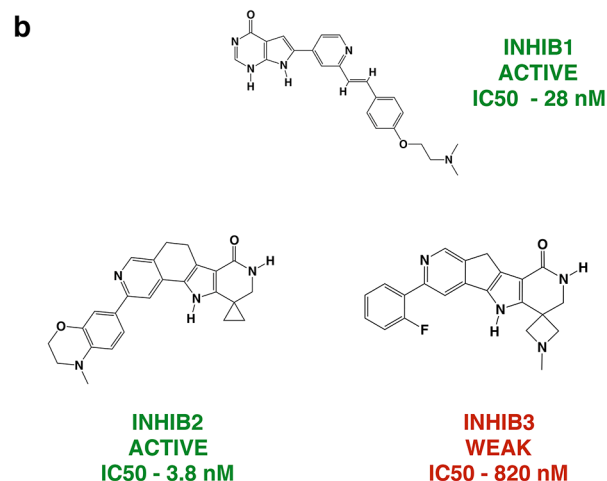
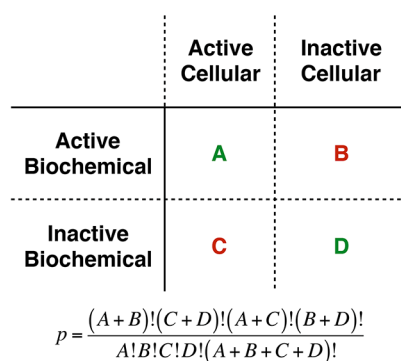
hit number	associated gene/MOA	Pubchem CID	SMILES	common name
1	Broad spectrum kinase inhibitor	44259	<chem>CN[C@@H]1C[C@H]2O[C@@](C)([C@@H]1OC)[N]3C4=CC=CC=C4C5=C6CNC(=O)C6=C7C8=CC=CC=C8[N]2C7=C35</chem>	Staurosporine
2	Viral protein inhibitor	148192	<chem>COC(=O)N[C@H](C(=O)N[C@H](CC1=CC=CC=C1)[C@@H](O)CN(CC2=CC=C(C=C2)C3=CC=CC=N3)NC(=O)[C@@H](NC(=O)OC(C)C(C)C(C)C)</chem>	Atazanavir
3	CYTH2; ARF1	5287620	<chem>C[C@H]1CCC/C=C/[C@@H]2[C@H](O)[C@H]2[C@H](O)C=C(C(=O)O1)</chem>	Brefeldin A
4	SSTR3	9910573	<chem>CCOC1(COCC)N[C@H](CC2=C1[NH]C3=CC=CC=C23)C4=NC=C([NH]4)C5=CC=CC=C5</chem>	CHEMBL2069501
5	EGFR; MUSK	11350462	<chem>C[C@@H](NC1=NC=NC2=C1C=C([NH]2)C3=CC=C(C4CCNCC4)C=C3)C5=CC=CC=C5</chem>	SCHEMBL3840840
6	AURKB; FLT3; AURK A	11675222	<chem>COC1=CC(=CC(=C1OC)NC2=CC(=O)C3=C(N)C4=CC=CC=C34</chem>	SCHEMBL4518219
7	ZAP70	11589703	<chem>NC1=C(C)C=CC(=C1)NC2=NC=CC(=N2)NC3=C(C(=CC(=O)C)S(N)(=O)=O</chem>	SCHEMBL1131002
8	ZAP70	11201568	<chem>NC1=C(C)C=CC(=C1)NC2=NC=CC(=N2)NC3=C(C4=C(OCCO4)C=C3)S(N)(=O)=O</chem>	SCHEMBL1131663
9	Natural product antibiotic	34230	<chem>CO[C@H]1C[C@@H](C[C@H]2CC[C@H](C)[C@@H](O2)[C@@H](C)C(O)=O)[C@]3(O[C@]3(O[C@H]3C)[C@H]4CC[C@](C)(O4)[C@@H]5O[C@H](C[C@H]6O)[C@@](O)(CO)[C@H](C)[C@@H]6C)[C@H]1C</chem>	Nigericin
10	ABL1; ABL2; SRC; CS K; YES1	10302451	<chem>CN1CCN(CCOC2=CC3=C(C(=NC=N3)NC4=C(C)C=CC5=C4OCOS)C(=C2)OC6CCOCC6)CC1</chem>	Saracatinib
11	HSPB1; MAPKAPK 2; AURKA; TNF	16119710	<chem>O=C1N=CNC2=C1C=C([NH]2)C3=CC(=NC=C3)/C=C/C4=CC=C(C5CCOCC5)C=C4</chem>	Pyrrolo-pyrimidone, 16
12	MAPKAPK2; AURK A; TNF	16119021	<chem>CN(C)COC1=CC=C(C(=O)C=C1)/C=C/C2=NC=CC(=C2)C3=CC4=C(NC=NC4=O)[NH]3</chem>	Pyrrolo-pyrimidone, 17
13	CASR	24753708	<chem>COC[C@H]1C(=NC2=C(C(=CC(=C12)OC)CC3=C(N=CC=C3)S)(C(=O)=O)C(F)F)C4=CC=C(C(=O)C(C)C</chem>	SCHEMBL2972172
14	JAK2	16722832	<chem>CN1CCN(CCI)C2=CC=CC=C(C(=N3)NC4=CC(=CC=C4)S)(=O)NC(C)(C)C=C2</chem>	TG101209
15	JAK2	46398810	<chem>FC1=C(CN2CCOCC2)C(=CC(=C1)C3=C4N=C(C(=NC4=CC=C3)C5=C(N)C6CCNCC6)F</chem>	NVP-BSK805
16	JAK2	57820201	<chem>C[C@H]1CN(C[C@H](C)N1)C2=NC=C(NC3=NC=C4C=C(C(=C(CN6COCOC6)C(=C5)F)C4=N3)C=C2</chem>	SCHEMBL1655083
17	MAPKAPK2	42646698	<chem>CN1CC2(CNC(=O)C3=C2[NH]C4=C3CC5=C(N=C(C(=C4)C6=CC=CC=C6)C1</chem>	CHEMBL1233942
18	FLT3;PRKCK	9829523	<chem>CO[C@H]1[C@@H](C[C@H]2O[C@]1(C) [N]3C4=CC=CC=C4C5=C6CNC(=O)C6=C7C8=CC=CC=C8[N]2C7=C35)N(C(=O)C9=CC=CC=C9</chem>	Midostaurin
19	KIT	24897305	<chem>CN1CCN(CCI)C2=CC=C(C(=C2)C(=O)NC3=CC(=C(C)C=C3)NC4=NC=CC(=N4)C5=CN=C(C)C=C5</chem>	CHEMBL1079113
20	JAK1; JAK2; TYK2	25062766	<chem>O=C(NCC#N)C1=CC=C(C(=C1)C2=NC(=NC=C2)NC3=CC=C(C(=C3)N4CCOCC4</chem>	Cyt387
21	AXL; MET	25166183	<chem>COC1=C(OCCN2CCOCC2)C=CC(=C1)C3=CC(=C(N)C(=N3)C4=NC5=C([NH]4)C=C(F)C=C5</chem>	SCHEMBL4009811
22	JAK3	46224516	<chem>CCN(C)C1CCCC(m1)j4nc(N2ccc(cc2)N3CCOCC3)nc5NC=Ne45</chem>	UNC0638
23	EHMT2	58973123	<chem>COC1=C(OCCN2CCOCC2)C=C3N=C(C(=N4CCN(CCC4)C(C)C)C3=C1)C5CCOCC5</chem>	SCHEMBL3233455
24	RAF1; BRAF	10022738	<chem>COC1=CC(=N/C1=C1C2NC(C)=CC=2C)C4=C(C3=CC=CC=C3)C4=C(C(=O)NC5=CC=CC(=C5)C(F)F</chem>	Obatoclax
25	BCL2; BCL2L2	49840814	<chem>COC1=CC(=N/C1=C1C2NC(C)=CC=2C)C4=C(C3=CC=CC=C3)C4=C(C(=O)NC5=CC=CC(=C5)C(F)F</chem>	Kinome_638
26	CCNE2	10022738	<chem>C[C@H]1CN(CCO1)C2=NC3=C(C(=C2)C(=NC=C3)NC4=CC(=C(C)C)C5=NC=C([NH]5)C6=CC=CC=C6</chem>	CHEMBL2160067
27	SMO	49840814	<chem>C6=CC=CC=C6</chem>	
28	PLK1	11364421	<chem>CC(C@H)1N(C2CCOCC2)C3=NC(=NC=C3N(C)C1=O)NC4=C(O)C=C(C(=O)C(=O)NC5CCN(C)CC5</chem>	BI 2536
29	CNR1	11316919	<chem>CC(F)CNC1CCOC2=C([N](N=C2C1=O)C3=CC=CC=C3C)C4=CC=C(C)C=C4</chem>	PF-514273
30	DGAT1	25235948	<chem>CC1=NC=C(NCC)N=C(O2)C3=CC=C(C(=C3)N=C([NH]4)C5=C(C)C=CC=C5C)C=C1</chem>	SCHEMBL1251920
31	CDK4	44819306	<chem>CN(C)C1CCN(CCI)C2=CC=CC=C(C(=O)C(=C4)C=C(C(=O)NC5=CC=CC(=C5)C(F)F)C4=N3)C=C2</chem>	SCHEMBL303554
32	KEAP1; IKKBK	400769	<chem>COC(=O)[C@]12CCCC(C)C[C@H]3C(=O)C=C4[C@@](C)(CC[C@H]5C(C)C(=O)C(=C[C@]45C)C#N)[C@]3(C)CC2</chem>	Bardoxolone methyl
33	TLR7; TLR8; TLR9	25105690	<chem>COC1=C(O)C=C2C(=NC(=NC2=C1)C3=CC=C(C(=C3)N4CCN(C)CC4)NCCN5CCOCC5</chem>	CHEMBL2144205
34	MERTK	9863278	<chem>CCCCNc3ccc2C(=NN([C@@H]1CC[C@H](O)CC1)c2n3)c4ccc(cc4)S(=O)(=O)N5CCOCC5</chem>	
35	SYK	9863278	<chem>CN(C(C)=O)C1=CC=C(NC2=NC3=C([NH]C=N3)C(=N2)NC4CC(C)C=C1</chem>	SCHEMBL1223740
36	PTK2		<chem>COCCO6cccc(Nc5ncc(Cl)c(Nc1ccc(cc2CCN(C)C(=O)c12)N3CCC(CC3)N4CCN(C)CC4)n5)c(c6)OC</chem>	

Table 2. continued

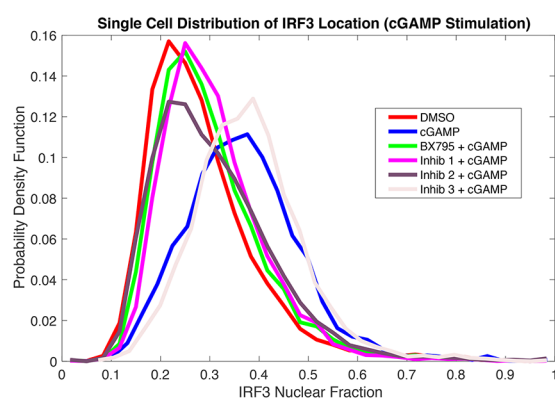
hit number	associated gene/MOA	Pubchem CID	SMILES	common name
37	MC4R; MC3R; MCSR	9938402	<chem>C[C@H]1C[C@@H](NC(=O)[C@H]2CC3=CC=CC=C3CN2)C(=O)N4CCC(CC4)C([N]5C=NC=N5)C6CCCC6)C=C1</chem>	THIQ
38	Natural product antibiotic		<chem>CC[C@H]1(C)[C@H](O1)[C@]3(C)CC[C@]2(C)[C@H](O)[C@H](O2)[C@H](C)[C@H](OC)[C@H](C)C(O)O3[C@H]4O[C@H](C[C@H]4C)[C@H]5O[C@@](O)(CO)[C@H](C)C[C@H]5C</chem>	Monensin
39		84815	<chem>CSCC[C@H](N)C(O)=O</chem>	D-methionine
40	Natural product antibiotic	11104823	<chem>COC1=CC=CC2=C1C(=C[NH]2)C[C@H]3NC(=O)[C@H](CC4=C[NH]C5=CC=CC=C45)NC(=O)C6=CSC(=N6)[C@H](C)NC(=O)CN(C)C(=O)C(=C)NC(=O)[C@H](C)NC(=O)CNC3=O</chem>	SCHEMBL16509614
41	ATP6 VIA	INTERNAL		
42	ATP6 VIA	INTERNAL		
43	PRKCH	INTERNAL		
44	GPR39	INTERNAL	<chem>CC(C)N1CCN(CC1)C6nc(C2C(=O)NC(=O)C=2C3=CNc4cccc34)c5cccc5n6</chem>	
45	TEK	INTERNAL	<chem>CN1CCN(CCC1)[C@H]2CC[C@H](CC2)N6C=C(c4ccc(NS(=O)(=O)C3=CC=CC=C3)c(F)c4)c5c(N)ncnc56</chem>	CHEMBL1089773
46	JAK1; JAK2	4686529	<chem>CN1CCN(CCC1)C2=CC=C(C(=C2)C3=NC4=C(C=CC=C4N=C3)C5=CC(=C(CN6COCOC6)C(=C5)F)F</chem>	CHEMBL3338839
47	ROCK1; ROCK2	91758287	<chem>C1CN(CCN1)C2=NC(=NC3=C2C=CN=C3)C4=C(CS=C([NH]N=C5)C=C4</chem>	Nintedanib
48	FGFR3; PDGFRA; PDGFRB; KDR; FLT4; FGFR1; FLT1	9809715	<chem>COC(=O)C1=C(C2=C(C=C1)\C(C(=O)N2)=C(\NC3=CC=C(C(=C3)N(C)C(=O)CN4CCN(C)CC4)C5=CC=CC=C5</chem>	
49	EHMT2; EHMT1	25150857	<chem>COC1=C(OC)C=C2C(=NC(=NC2=C1)N3CCCN(C)CC3)NC4CCN(CC4)CC5=CC=CC=C5</chem>	BIX-01294
50	ALK; NTRK1; NTRK2; NTRK3	44470247	<chem>O[C@H]1CCN(C1)C2=NC=CC(=N2)C3=NC(=CC=C3)C4=CN=C5C=CC(=N[N]45)N6CCC[C@H]6C7=CC(=CC=C7)F</chem>	SCHEMBL1430945
51	DYRK1A; GSK3B	INTERNAL		
52	RXRG; RXRB; RXRA	10360455	<chem>CC1=CC2=C(C=C1C(=O)C3=NC=C(C(=O)C)C(C)C)C(C)C(C)C(C)C</chem>	
53	GABBR1; GABBR2	44601	<chem>NC[C@H](CC(O)=O)C1=CC=C(C1)C=C1</chem>	
54	ATP6 VIA	INTERNAL		
55	PP1B; PPIB; PPIF	INTERNAL		Bafilomycin derivative

^aCompounds 1–38 compounds were selected for secondary screening based on availability and biological interest. Bafilomycin and concanomycin were also included as replacements for the three ATP6 VIA inhibitors.

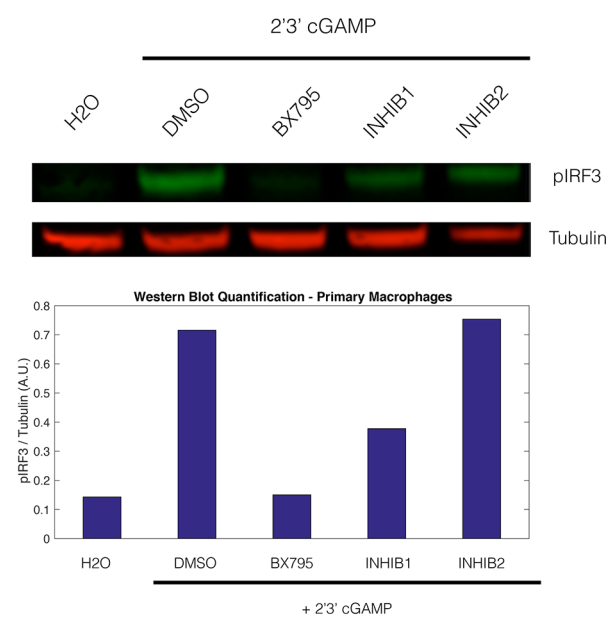
a Target enrichment for kinase inhibitors



c



d



e

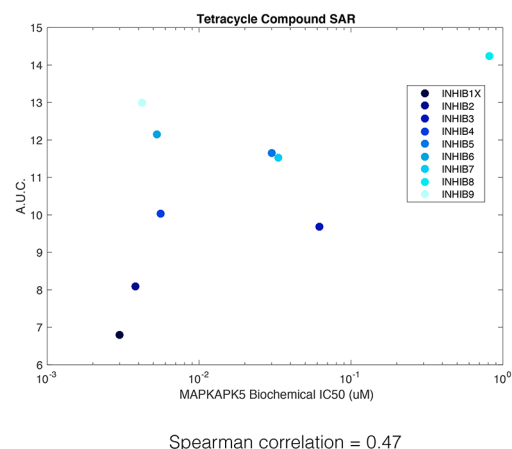
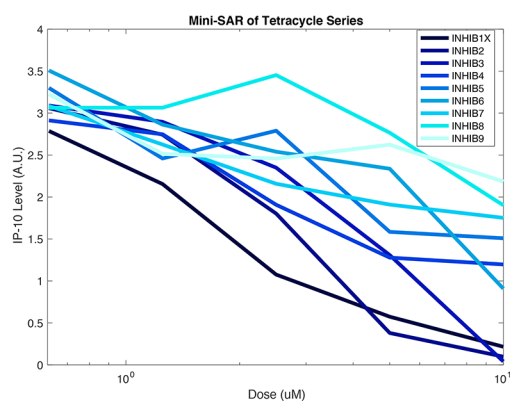


Figure 6. Retest of MAPKAPK5 inhibitors. (a) Enrichment strategy to identify relevant kinase targets in inhibitor list. (b) Structures of MAPKAPK5 inhibitors. INHIB1 and INHIB2 are active, while INHIB3 has much weaker affinity for MAPKAPK5. (c) Retest of INHIBS 1, 2, and 3 in imaging assay in a single donor. Shown is the IRF3 distribution in cells treated with inhibitor (10 μ M, 2 h pretreatment) and 2'3' cGAMP (75 μ M, 2 h stimulation). (d) Western blot measuring IRF3 phosphorylation (Ser396) after 4 h stimulation with 2'3' cGAMP (62.5 μ M) in the presence or absence of inhibitor (10 μ M). Cells were pretreated with inhibitor for about 2 h. Shown below is quantification of pIRF3 levels normalized to tubulin. (e) Mini-SAR of nine tetracycline (INHIB2-like) MAPKAPK5 inhibitors. IP-10 levels are measured (left), and biological activity is plotted against MAPKAPK5 IC₅₀ (right).

ascribed target(s). We examined data from all kinase inhibitors, both hits and nonhits, and calculated an enrichment score for each kinase gene in the active compound list, using hypergeometric enrichment. We classified compounds as active or inactive in cellular assays based on their IRF3 inhibition scores and classified them as active or inactive against a kinase target by examining available biochemical data (Figure 6a). A major challenge was that not all inhibitors have been comprehensively profiled, and available biochemical data are subject to unknown errors. To simplify the analysis, we made the assumption that if biochemical data on a compound are missing, the molecule is inactive against the target. With this limitation in mind, we computed an enrichment score for each kinase gene,²⁸ by calculating the p-value based on 2×2 contingency table. For each kinase, we look at the number of inhibitors that are either (A) active biochemically and active in cell-based assays, (B) active biochemically but inactive in cell-based assays, (C) inactive biochemically and active in cell-based assays, or (D) inactive biochemically and inactive in cell-based assays. The number of inhibitors in groups A and D enrich for the kinase of interest, while the numbers in C and D de-enrich (Figure 6a).

TBK1 was among the top enriched genes in this analysis (#8, Supporting Information Figure 6), as were ALK and AMPK (#7 and #17), two kinases that have been proposed as STING pathway regulators.^{29–31} To focus on novel kinases, we removed compounds with known activities against TBK1 and reran enrichment. MAPKAPK5 emerged as a particularly promising kinase required for STING-pathway activity. First, MAPKAPK5 passed the hypergeometric enrichment test (p-value < 0.005, #18). A second, nonbinary method described in the supplement, in which partial correlations are computed between the IRF3 and biochemical inhibition score, also yielded a high score for MAPKAPK5. MAPKAPK5 was inhibited by five probes in our screen, which was favorable from a practical perspective for subsequent experiments. MAPKAPK5 is expressed in macrophages, appears to be an inflammatory kinase, and has been reported to phosphorylate IRF3 *in vitro*.³² MAPKAPK5 has been considered as a therapeutic target for rheumatoid arthritis,³³ yet its overall biological function has not been explored in depth. A recent report also suggests that it may be involved in the inflammatory pathology of Alzheimer's disease.³⁴

Diverse MAPKAPK2/5 Inhibitors Block STING Pathway Activation. In Table 2, hits 11, 12, and 17 all inhibit MAPKAPK5. However, our biochemical IC₅₀ data also indicated that they inhibit MAPKAPK2, a closely related kinase which has been implicated in TLR4 signaling.³⁵ While not enriched in our initial analysis, MAPKAPK2 is a potent target of these compounds, and given its previously described role in TLR signaling,³⁵ we thought it was plausible that it could also be an efficacy target of the compounds we identified. Indeed, it seemed possible that dual inhibition of MAPKAPK2 and MAPKAPK5 could be required to block the STING pathway. In subsequent assays, we used compound 11 and a more potent tetracycline analog of compound 14 (Figure 6b, INHIB1 and INHIB2) as probes to inhibit MAPKAPK2/5. We also included INHIB3 (Figure 6b), a tetracycline compound that resembles INHIB2 but has much weaker affinity for MAPKAPK2/5.

We reconfirmed that INHIB1 and INHIB2 were active in blocking IRF3 nuclear translocation induced by 2'3'-cGAMP in primary human macrophages. Cells from this particular donor did not respond strongly to 2'3'-cGAMP, but examination of IRF3 nuclear fraction at the single cell level showed that

INHIB1, INHIB2, and BX795 phenocopied untreated cells, while INHIB3, the much weaker MAPKAPK5 inhibitor, phenocopied 2'3'-cGAMP treated cells (Figure 6c). Additionally, while BX795 treatment completely ablated IRF3 phosphorylation at Ser396, INHIB1 had a slight effect while INHIB2 had no effect on phospho-IRF3-Ser396 levels, respectively (Figure 6d). Further replicates are needed to determine if the reduction by INHIB1 is physiologically relevant; however, we performed a similar experiment in THP1 cells and saw no effect on phospho-IRF3 levels (Supporting Information Figure 7). Taken together, these data indicate that INHIB1 and INHIB2 are active in blocking IRF3 nuclear translocation but are unlikely to be active against the main STING pathway kinase TBK1.

SAR against MAPKAPK2/5 Support Their Involvement in the STING Pathway. Next we tested a panel of nine tetracyclines, structurally similar to INHIB2 (Supporting Information Figure 8), for their effect on the STING pathway, using ELISA to determine the extent of IP-10 induction. The nine tetracyclines had a range of inhibitory activities against the STING pathway, consistent with their respective MAPKAPK5 biochemical affinities (Figure 6e). As mentioned above, these compound also inhibited MAPKAPK2, and the biological and chemical activities were also weakly correlated (Supporting Information Figure 9). No biologically active compounds were inactive against MAPKAPK2/5, so neither of these kinases can be ruled out as the relevant efficacy target for the tetracycline-like compounds.

Toxicity is unlikely to account for the inhibitory activities of INHIB1 and INHIB2. We measured inhibition of the STING pathway by INHIB1 and INHIB2, using IP-10 ELISA in a different donor, and also in parallel ran a Cell-Titer-Glo (CTG) assay on the same plate (Supporting Information Figure 10a). Both INHIB1 and INHIB2 blocked IP-10 secretion in this donor. By Cell-Titer-Glo, INHIB1 showed no toxicity, and INHIB2 only showed toxicity at higher doses. Examination of the dose response curves shows that INHIB2 reduces pathway activation around 1–5 μM , with little effect on the CTG count. Additionally, in the aforementioned mini-SAR experiment, we also stained for nuclei after collecting the media for ELISA (Supporting Information Figure 10b). For INHIB2, the nuclei count is reduced by less than 10% at the highest dose. Taken together, while INHIB2 shows some toxicity, we think that it is not significant enough to fully account for its biological activity.

As mentioned before, a key challenge faced was that not all inhibitors were comprehensively profiled across the kinome. Biochemical IC₅₀ data for the inhibitors against several kinases were missing. To provide a comprehensive kinase inhibitor selectivity profile, we performed a lysate-based chemical proteomics experiment that utilized pan-kinase inhibitors coupled to sepharose beads to assay the expressed kinome of THP1 cells.^{36,37} Preincubation of INHIB1 or INHIB2 blocked the enrichment of MAPKAPK5, but not TBK1 or any other kinase that has been definitively linked to the STING pathway. However, while the compounds were relatively clean, they were not sufficiently selective to decisively implicate MAPKAPK2/5 in STING signaling (Supporting Information Figure 11)

DISCUSSION

We developed high content assays for assessing activation of STING and other innate immune pathways, by measuring IRF3 and NF κ B nuclear translocation. The high content screening assay we developed has many advantages and may find other

uses. It can be performed in a high-throughput 1536-well format, requires a small number of cells per well, and is compatible with any adherent cell type including primary human cells. No external marker or reporter is required, and use with difficult to culture cells (i.e., dendritic cells) and other pathways (i.e., STAT1) seems feasible, as so long as validated antibodies are available. A key challenge we faced in the case of primary macrophages was donor-to-donor variability, which is potentially an issue in any screen using fresh primary cells. For future work, we recommend carefully characterizing this variable in all subsequent experiments. This is particularly important in development of any potential therapeutics. For controls, outlier wells presented another challenge, and it is thus important to include several replicates for controls, and also to screen in duplicates if possible. Lastly, screening in dose was also very important. The diverse small molecules in the library had a wide range of active concentrations, and a single dose would not be able to account for all of them.

In the activator screen, we identified multiple compounds that cause IRF3 and NFkB nuclear localization but found that most did not induce downstream gene expression programs. This is a significant liability of the assay. The existence of such hits reveals new ways to move IRF3 and NFkB into the nucleus without activating gene expression, which may be of use for dissecting mechanisms of translocation in greater detail. In a secondary screen, the Zn²⁺ chelator TPEN induced secretion of IP-10 to levels comparable to those of 2'3'-cGAMP and LPS. The effect was donor-specific, possibly because of a narrow concentration range between activating IP-10 production and killing the cells. This reduced the value of TPEN as a tool compound, and it seems highly unlikely that TPEN has therapeutic value.

The antagonist screen identified numerous STING pathway antagonists with reasonable concordance between the primary screen and follow-up assays. Kinase inhibitors dominated the list of hits, and our follow up analysis focused on a set of MAPKAPK2/5 inhibitors, from which we tried to identify an efficacy target using SAR and chemical proteomics. Chemical proteomic data confirmed that these compounds selectively bound to MAPKAPK5, and further, SAR suggested that MAPKAPK5 is the likely efficacy target of these inhibitors, though we cannot rule out MAPKAPK2. Establishing whether the mechanism of the inhibitors is certainly due to MAPKAPK5 or MAPKAPK2 or both would be difficult in primary macrophages. The ideal solution would be to perform genetic knockouts, or transfection with inhibitor-resistant mutants, but doing so in primary human immune cells is difficult. An alternative would be to use cell lines, though many of the cell lines with active STING pathways, such as THP1, are also quite difficult to manipulate genetically. Moreover, if a KO in a cell line did not show any phenotype, this could be due to cell-type specificity, which has already been reported in the context of the STING pathway.¹⁶ The tetracycline scaffold, which achieved potent inhibition of MAPKAPK5 and IP-10 secretion in human macrophages, could potentially be further developed as a novel anti-inflammatory drug candidate. Such compounds are active against the STING pathway without noticeably inhibiting TBK1. Many inflammatory diseases have been characterized by overactive STING signaling, and our work suggests that there are druggable targets, particularly kinases, to consider beyond cGAS, STING, and TBK1.

METHODS

Primary Screening Assay. Primary human CD14⁺ monocytes (Lonza) were seeded into 1536 well plates (Greiner Lo base) at a density of 1250 cells/well. Monocytes were differentiated into macrophages by adding 100 ng/mL of recombinant human M-CSF (Pepro-Tech, Catalog # 300-25) into the cell media (RPMI, 10% FBS, 1% P/S) for 1 week. Media were replaced after 3 days of differentiation. After 1 week, media were washed out and replaced with just RPMI, 10% FBS, and 1% P/S. In the activator screen, cells were treated with the compound for 4 h. In the inhibitor screen, cells were pretreated with the compound for 4 h, and subsequently treated with 100 μM 2'3' cGAMP for 4 h, still in the presence of the compound. In both screens, cells were fixed with 4% PFA for 30 min, washed with PBS, and then blocked, permeabilized, and stained overnight at RT. The buffer for staining was adjusted for a final well concentration of 2% BSA and 0.125% Triton-X-100 in PBS. IRF3 XP antibody (Cell Signaling, 11904 T) and NFkB antibody (Santa Cruz, sc-8008) were adjusted to a final dilution of 1:400.

After primary antibody staining, plates were washed in PBS and then stained for 2 h at RT, with goat antirabbit Alexa Fluor 488 (Thermo Fisher, A-11034), donkey antimouse Alexa Fluor 647 (Thermo Fisher A-31571), and DAPI. Final dilution of the antibody was 1:400, and DAPI concentration was 0.1 μg/mL. The buffer was the same as before (2% BSA, 0.125% Triton-X-100 in PBS). Plates were then washed and imaged on an InCell 3000. The FITC channel was used to capture Alexa 488 stain, and Cy5 was used to capture Alexa 647 channel.

High Content Analysis. Image processing was performed on the Columbus HMS server. To identify cells, a mask was first used to identify nuclei from the DAPI channel. Cytoplasmic spaces were then identified by segmenting areas of Alexa-488 and Alexa-647 staining (outside each nuclei) that scored above the background. From the image processing, 36 features were computed.

(1) IRF3 intensity and localization (three features: nuclear fraction, nuclear IRF3 intensity, cytoplasm IRF3 intensity):

(a) Nuclear IRF3 = (size_nucleus) × (mean_FITC_nuclear − mean_FITC_background)

(b) Cytoplasmic IRF3 = (size_cytoplasm_FITC) × (mean_FITC_cytoplasm − mean_FITC_background)

(c) Nuclear fraction = Nuclear IRF3 / (Nuclear IRF3 + Cytoplasmic IRF3)

(2) NFkB intensity and localization (three features: Nuclear Intensity, Cytoplasmic Intensity, Fraction Nuclear). Parameters calculated as above.

(3) DAPI intensity (one feature)

(4) IRF3 nuclear texture (four Haralick features: Correlation, Contrast, Sum Variance, Homogeneity)

(5) IRF3 cytoplasmic texture (four Haralick features)

(6) NFkB nuclear texture (four Haralick features)

(7) NFkB cytoplasmic texture (four Haralick features)

(8) DAPI nuclear texture (four Haralick features)

(9) IRF3 morphology (three features using cytoplasm channel – Area, Roundness, Length to Width Ratio)

(10) NFkB morphology (three features using cytoplasm channel – Area, Roundness, Length to Width Ratio)

(11) DAPI morphology (three features in the nucleus – Area, Roundness, Length to Width Ratio)

Selection of Hits. Activator screen: Using the above features, a quadratic-kernel support vector machine was trained using MATLAB Machine Learning Toolbox. The supervised learning approach was based on data from control wells: H₂O, 2'3' cGAMP, 3'3' cGAMP, LPS, and CL075. Training was done with 10-fold cross validation. After training, the SVM was used to classify every well in the screening assay. For every compound, we considered 12 wells (six doses, from 10 μM to 31.6 nM at half-log titration, in duplicate). Any compound that was classified as 2'3' cGAMP at least twice in the 12 wells was selected for follow up.

Inhibitor screen: Data from 2'3' cGAMP and H₂O wells were aggregated, and PCA was used to reduce dimensionality to six features

(~90% of variability). In this transformed space, a Mahalanobis distance between the H₂O control group and every compound was treated well. A distance threshold was set by the 90% quantile of the BX795 + 2'3' cGAMP control.

A compound was selected if either (1) out of 12 wells (six doses from 10 μ M to 31.6 nM, in duplicate), at least two wells were close enough to the H₂O control group OR (2) out of 14 wells (seven doses from 31.6 μ M to 31.6 nM, in duplicate), at least three wells were sufficiently close to the H₂O control group.

Secondary Screening Assay. CD14 monocytes were seeded in a 96 well plate, at approximately 50 000 cells/well. Cells were differentiated as above. In activator secondary screen, cells were treated with the compound for 11 h, at six doses in duplicate, and IP-10 levels were measured using an ELISA kit (R&D DY266-05). In the inhibitor secondary screen, cells were pretreated with compound for 1.5–2 h and then treated with 40 μ M 2'3' cGAMP for approximately 17 h. IP-10 levels were again measured with an ELISA kit (R&D DY266-05). The TNF α data in the supplement were also obtained using an ELISA kit (R&D DY210-05)

Additional Follow-Up. Any immunofluorescence or IP-10 ELISAs were done as above. Thp1-ISG-LUCIA and RAW-ISG-LUCIA cell lines were obtained from Invivogen. LUCIA assays were performed as described in the manufacturer's protocol. For Western blots, the phospho-IRF3 antibody was obtained from Cell Signaling (4947S), and the tubulin antibody was obtained from Sigma (T9026). We performed near-IR Western blotting, using an Odyssey blocking buffer (LI-COR, P/N 927-40100) and following the LI-COR Odyssey near-IR Western blot protocol. Secondary antibodies were Goat Anti-Rabbit 800 DyLight (Thermo, 35571) and Goat Anti-Mouse 680 DyLight (Thermo 35518), used at 1:15 000 dilution.

For Supporting Information Figure 11, THP1 cells were first differentiated using phorbol 12-myristate 13-acetate (PMA) to make them more macrophage-like and adherent. Cells were treated with PMA (200 ng/mL) for approximately 18 h, and media were subsequently washed out with plain cell culture media.

Cell-titer-glo assay (Supporting Information Figure 10) was performed as per the manufacturer's protocol.

Sources and Isolation of Macrophages. For the primary screen, CD14+ monocytes were ordered directly from Lonza. For all secondary screening and follow up, peripheral blood mononuclear cells (PBMCs) were first isolated from leukapheresis donors (Boston Children's Hospital), using a standard protocol.³⁸ CD14+ monocytes were subsequently isolated using a CD14+ antibody and magnetic sorting (MACS, Miltenyi Biotec). Cells were not further characterized.

Different donors were used in all screens and assays (primary activator and inhibitor screens, secondary screens, follow-up). For each assay, we strived to use a single donor for each assay. However, in the primary screens, in which we ordered cells directly from Lonza, we did not have enough cells from a single donor to cover all assay plates. As a result, we had to use a mixture of cells that came predominantly from one donor (~75%). Different donors were used for the activator and inhibitor screens.

Cherry-Picked Compounds for Follow Up. Our primary screen was conducted at Novartis Institutes for Biomedical Research (NIBR), while our secondary screening and follow up was conducted at Harvard Medical School (HMS). All molecules plated in the initial screen were verified for chemical purity using liquid chromatography–mass spectrometry (LC-MS).

All compounds selected for follow-up at HMS were public compounds; however, several were not available from reliable, commercial sources. As a result, we requested about 2/3 of the hits from NIBR. The purity of these hits was verified using LC-MS. For practical reasons, we ordered the remaining 1/3 of hits from standard chemical sources. The purity of these hits was verified by the vendor, but not at HMS.

Kinase Inference Computations. Biochemical IC₅₀ data for every compound were assembled into a matrix, where each row represents a compound and each column represents a kinase. Each element of the matrix contains the measured biochemical IC₅₀, taken from internal data, for the specified inhibitor and kinase target. If a

kinase was not profiled for a given inhibitor, it was assumed inactive by giving it a biochemical IC₅₀ of 100 μ M.

For hypergeometric enrichment, an inhibitor was deemed biochemically active in a well if the dose was 10 times greater than the biochemical IC₅₀. This is a free parameter, and it is to account for the fact that inhibitors typically must be used at doses greater than their biochemical profile, for reasons such as cell permeability, transport, metabolism, etc. Biological activity was determined by the IRF3 nuclear localization score. An inhibitor was deemed biologically active if the IRF3 nuclear localization score was within two standard deviations of the H₂O control. The p values for all expressed kinases were then computed using the contingency table in Figure 6a. We subsequently removed TBK1-active compounds (compounds with IC₅₀s less than 1 μ M) and reran enrichment.

We note that p values in this test were used primarily to rank the kinases, and one must be cautious in interpreting the actual value itself, due to a false discovery rate, for which we did not correct. In particular, the hypergeometric test can enrich several genes strongly, as our biochemical IC₅₀ data are complete, and some kinases can have several data points in group D (biologically inactive and biochemically inactive), which enriches for the gene. Additionally, several genes may be enriched simultaneously, because of transitive effects, e.g., kinases commonly inhibited by the same inhibitors.

We also calculated partial correlations between the IRF3 score and biochemical inhibition score. This approach is described in Supporting Information Figure 6.

Chemoproteomics Methods. Chemoproteomics were performed as in ref 35. Immobilized pan-kinase inhibitors (compound-2 from ref 35 and VI16832 from ref 36) were combined in a 1:1 ratio and used to pull down kinases from THP1 cell lysate.

■ ASSOCIATED CONTENT

■ Supporting Information

The Supporting Information is available free of charge on the ACS Publications website at DOI: 10.1021/acscchembio.7b01060.

Supporting Figures 1–11 as well as structures of all molecules used in secondary screenin (PDF)

■ AUTHOR INFORMATION

Corresponding Author

*E-mail: peterkoch@fas.harvard.edu.

ORCID

Peter D. Koch: 0000-0001-8312-1657

Jason R. Thomas: 0000-0001-7502-3600

Funding

This work was supported by National Institutes of Health grant U54-HL127365.

Notes

The authors declare the following competing financial interest(s): Howard Miller, Gary Yu, John Tallarico, Yuan Wang, Yan Feng, and Jason Thomas are employees of Novartis Institutes for Biomedical Research. Nathan Ross is a former employee of Novartis Institutes for Biomedical Research.

■ ACKNOWLEDGMENTS

We thank Hua Wu, Sanghee Lee, and Zoltan Maliga for helpful advice and discussion of this work.

■ REFERENCES

(1) Kawai, T., and Akira, S. (2011) Toll-like receptors and their crosstalk with other innate receptors in infection and immunity. *Immunity* 34, 637–650.

- (2) Kawai, T., and Akira, S. (2006) Antiviral signaling through pattern recognition receptors. *J. Biochem.* *141*, 137–145.
- (3) Cai, X., Chiu, Y. H., and Chen, Z. J. (2014) The cGAS-cGAMP-STING pathway of cytosolic DNA sensing and signaling. *Mol. Cell* *54*, 289–296.
- (4) Liu, Y., Jesus, A. A., Marrero, B., Yang, D., Ramsey, S. E., Montealegre Sanchez, G. A., Tenbrock, K., Wittkowski, H., Jones, O. Y., Kuehn, H. S., Lee, C. R., DiMattia, M. A., Cowen, E. W., Gonzalez, B., Palmer, I., DiGiovanna, J. J., Biancotto, A., Kim, H., Tsai, W. L., Trier, A. M., Huang, Y., Stone, D. L., Hill, S., Kim, H. J., St. Hilaire, C., Gurprasad, S., Plass, N., Chapelle, D., Horkayne-Szakaly, I., Foell, D., Barysenka, A., Candotti, F., Holland, S. M., Hughes, J. D., Mehmet, H., Issekutz, A. C., Raffeld, M., McElwee, J., Fontana, J. R., Minniti, C. P., Moir, S., Kastner, D. L., Gadina, M., Steven, A. C., Wingfield, P. T., Brooks, S. R., Rosenzweig, S. D., Fleisher, T. A., Deng, Z., Boehm, M., Paller, A. S., and Goldbach-Mansky, R. (2014) Activated STING in a vascular and pulmonary syndrome. *N. Engl. J. Med.* *371*, 507–518.
- (5) Vermeire, J., Roesch, F., Sauter, D., Rua, R., Hotter, D., Van Nuffel, A., Vanderstraeten, H., Naessens, E., Iannucci, V., Landi, A., Wittkowski, W., Baeyens, A., Kirchhoff, F., and Verhasselt, B. (2016) HIV Triggers a cGAS-Dependent, Vpu- and Vpr-Regulated Type I Interferon Response in CD4(+) T Cells. *Cell Rep.* *17*, 413–424.
- (6) Yang, H., Wang, H., Ren, J., Chen, Q., and Chen, Z. J. (2017) cGAS is essential for cellular senescence. *Proc. Natl. Acad. Sci. U. S. A.* *114*, E4612–E4620.
- (7) Chaudhari, K., Rizvi, S., and Syed, B. A. (2016) Rheumatoid arthritis: current and future trends. *Nat. Rev. Drug Discovery* *15*, 305–306.
- (8) Weinmann, H. (2016) Cancer Immunotherapy: Selected Targets and Small-Molecule Modulators. *ChemMedChem* *11*, 450–466.
- (9) Zhang, X., Shi, H., Wu, J., Zhang, X., Sun, L., Chen, C., and Chen, Z. J. (2013) Cyclic GMP-AMP containing mixed phosphodiester linkages is an endogenous high-affinity ligand for STING. *Mol. Cell* *51*, 226–235.
- (10) Unterholzner, L. (2013) The interferon response to intracellular DNA: why so many receptors?.. *Immunobiology* *218*, 1312–1321.
- (11) Downey, C. M., Aghaei, M., Schwendener, R. A., and Jirik, F. R. (2014) DMXAA causes tumor site-specific vascular disruption in murine non-small cell lung cancer, and like the endogenous non-canonical cyclic dinucleotide STING agonist, 2'3'-cGAMP, induces M2 macrophage repolarization. *PLoS One* *9*, e99988.
- (12) Fu, J., Kanne, D. B., Leong, M., Glickman, L. H., McWhirter, S. M., Lemmens, E., Mechette, K., Leong, J. J., Lauer, P., Liu, W., Sivick, K. E., Zeng, Q., Soares, K. C., Zheng, L., Portnoy, D. A., Woodward, J. J., Pardoll, D. M., Dubensky, T. W., Jr., and Kim, Y. (2015) STING agonist formulated cancer vaccines can cure established tumors resistant to PD-1 blockade. *Sci. Transl. Med.* *7*, 283ra52.
- (13) Baguley, B. C. (2011) Preclinical efficacy of vascular disrupting agents in non-small-cell lung cancer. *Clin. Lung Cancer* *12*, 81–86.
- (14) McKeage, M. J., and Baguley, B. C. (2010) Disrupting established tumor blood vessels: an emerging therapeutic strategy for cancer. *Cancer* *116*, 1859–1871.
- (15) Yan, N. (2017) Immune Diseases Associated with TREX1 and STING Dysfunction. *J. Interferon Cytokine Res.* *37*, 198–206.
- (16) Mayer, T. U., Kapoor, T. M., Haggarty, S. J., King, R. W., Schreiber, S. L., and Mitchison, T. J. (1999) Small molecule inhibitor of mitotic spindle bipolarity identified in a phenotype-based screen. *Science* *286*, 971–974.
- (17) Perlman, Z. E., Slack, M. D., Feng, Y., Mitchison, T. J., Wu, L. F., and Altschuler, S. J. (2004) Multidimensional drug profiling by automated microscopy. *Science* *306*, 1194–1198.
- (18) Pryke, K. M., Abraham, J., Sali, T. M., Gall, B. J., Archer, I., Liu, A., Bambina, S., Baird, J., Gough, M., Chakhtoura, M., Haddad, E. K., Kirby, I. T., Nilsen, A., Streblow, D. N., Hirsch, A. J., Smith, J. L., and DeFilippis, V. R. (2017) A Novel Agonist of the TRIF Pathway Induces a Cellular State Refractory to Replication of Zika, Chikungunya, and Dengue Viruses. *mBio* *8*, e00452-17.
- (19) Khair, S., Lucas-Hourani, M., Nisole, S., Smith, N., Helynck, O., Bourguine, M., Ruffie, C., Herbeuval, J. P., Munier-Lehmann, H., Tangy, F., and Vidalain, P. O. (2017) Identification of a small molecule that primes the type I interferon response to cytosolic DNA. *Sci. Rep.*, DOI: 10.1038/s41598-017-02776-z.
- (20) Wang, Y., Cornett, A., King, F. J., Mao, Y., Nigsch, F., Paris, C. G., McAllister, G., and Jenkins, J. L. (2016) Evidence-Based and Quantitative Prioritization of Tool Compounds in Phenotypic Drug Discovery. *Cell Chem. Biol.* *23*, 862–874.
- (21) Kumar, K. P., McBride, K. M., Weaver, B. K., Dingwall, C., and Reich, N. C. (2000) Regulated nuclear-cytoplasmic localization of interferon regulatory factor 3, a subunit of double-stranded RNA-activated factor 1. *Mol. Cell. Biol.* *20*, 4159–4168.
- (22) Wang, Q., Liu, X., Cui, Y., Tang, Y., Chen, W., Li, S., Yu, H., Pan, Y., and Wang, C. (2014) The E3 ubiquitin ligase AMFR and INSIG1 bridge the activation of TBK1 kinase by modifying the adaptor STING. *Immunity* *41*, 919–933.
- (23) Tsuchida, T., Zou, J., Saitoh, T., Kumar, H., Abe, T., Matsuura, Y., Kawai, T., and Akira, S. (2010) The ubiquitin ligase TRIM56 regulates innate immune responses to intracellular double-stranded DNA. *Immunity* *33*, 765–776.
- (24) Brieger, A., Rink, L., and Haase, H. (2013) Differential regulation of TLR-dependent MyD88 and TRIF signaling pathways by free zinc ions. *J. Immunol.* *191*, 1808–1817.
- (25) Clark, K., Peggie, M., Plater, L., Sorcek, R. J., Young, E. R., Madwed, J. B., Hough, J., Mclver, E. G., and Cohen, P. (2011) Novel cross-talk within the IKK family controls innate immunity. *Biochem. J.* *434*, 93–104.
- (26) Blaauboer, S. M., Gabrielle, V. D., and Jin, L. (2014) MPYS/STING-mediated TNF-alpha, not type I IFN, is essential for the mucosal adjuvant activity of (3'-5')-cyclic-di-guanosine-monophosphate in vivo. *J. Immunol.* *192*, 492–502.
- (27) Gonugunta, V. K., Sakai, T., Pokatayev, V., Yang, K., Wu, J., Dobbs, N., and Yan, N. (2017) Trafficking-Mediated STING Degradation Requires Sorting to Acidified Endolysosomes and Can Be Targeted to Enhance Anti-tumor Response. *Cell Rep.* *21*, 3234–3242.
- (28) Polyakov, V. R., Moorcroft, N. D., and Drawid, A. (2014) Enrichment analysis for discovering biological associations in phenotypic screens. *J. Chem. Inf. Model.* *54*, 377–386.
- (29) Zeng, L., Kang, R., Zhu, S., Wang, X., Cao, L., Wang, H., Billiar, T. R., Jiang, J., and Tang, D. (2017) ALK is a therapeutic target for lethal sepsis. *Sci. Transl. Med.* *9*, ean5689.
- (30) Prantner, D., Perkins, D. J., and Vogel, S. N. (2017) AMP-activated Kinase (AMPK) Promotes Innate Immunity and Antiviral Defense through Modulation of Stimulator of Interferon Genes (STING) Signaling. *J. Biol. Chem.* *292*, 292–304.
- (31) Konno, H., Konno, K., and Barber, G. N. (2013) Cyclic dinucleotides trigger ULK1 (ATG1) phosphorylation of STING to prevent sustained innate immune signaling. *Cell* *155*, 688–698.
- (32) Newman, R. H., Hu, J., Rho, H. S., Xie, Z., Woodard, C., Neiswinger, J., Cooper, C., Shirley, M., Clark, H. M., Hu, S., Hwang, W., Seop Jeong, J., Wu, G., Lin, J., Gao, X., Ni, Q., Goel, R., Xia, S., Ji, H., Dalby, K. N., Birnbaum, M. J., Cole, P. A., Knapp, S., Ryazanov, A. G., Zack, D. J., Blackshaw, S., Pawson, T., Gingras, A. C., Desiderio, S., Pandey, A., Turk, B. E., Zhang, J., Zhu, H., and Qian, J. (2013) Construction of human activity-based phosphorylation networks. *Mol. Syst. Biol.* *9*, 655.
- (33) Andrews, M. J., Clase, J. A., Bar, G., Tricarico, G., Edwards, P. J., Brys, R., Chambers, M., Schmidt, W., MacLeod, A., Hirst, K., Allen, V., Birault, V., Le, J., Harris, J., Self, A., Nash, K., and Dixon, G. (2012) Discovery of a series of imidazopyrazine small molecule inhibitors of the kinase MAPKAPK5, that show activity using in vitro and in vivo models of rheumatoid arthritis. *Bioorg. Med. Chem. Lett.* *22*, 2266–2270.
- (34) Kim, Y., Kim, C., Son, S. M., Song, H., Hong, H. S., Han, S. H., and Mook-Jung, I. (2016) The novel RAGE interactor PRAK is associated with autophagy signaling in Alzheimer's disease pathogenesis. *Mol. Neurodegener.*, DOI: 10.1186/s13024-016-0068-5.
- (35) Ehrling, C., Ronkina, N., Bohmer, O., Albrecht, U., Bode, K. A., Lang, K. S., Kotlyarov, A., Radzioch, D., Gaestel, M., Haussinger, D.,

and Bode, J. G. (2011) Distinct functions of the mitogen-activated protein kinase-activated protein (MAPKAP) kinases MK2 and MK3: MK2 mediates lipopolysaccharide-induced signal transducers and activators of transcription 3 (STAT3) activation by preventing negative regulatory effects of MK3. *J. Biol. Chem.* 286, 24113–24124.

(36) Gower, C. M., Thomas, J. R., Harrington, E., Murphy, J., Chang, M. E., Cornella-Taracido, I., Jain, R. K., Schirle, M., and Maly, D. J. (2016) Conversion of a Single Polypharmacological Agent into Selective Bivalent Inhibitors of Intracellular Kinase Activity. *ACS Chem. Biol.* 11, 121–131.

(37) Daub, H., Olsen, J. V., Bairlein, M., Gnad, F., Oppermann, F. S., Korner, R., Greff, Z., Keri, G., Stemmann, O., and Mann, M. (2008) Kinase-selective enrichment enables quantitative phosphoproteomics of the kinome across the cell cycle. *Mol. Cell* 31, 438–448.

(38) Fuss, I. J., Kanof, M. E., Smith, P. D., and Zola, H. (2009) Isolation of whole mononuclear cells from peripheral blood and cord blood, *Current Protocols in Immunology*, Chapter 7, Unit 7.1, John Wiley & Sons, Inc., Hoboken, NJ, DOI: [10.1002/0471142735.im0701s85](https://doi.org/10.1002/0471142735.im0701s85).